J. Phys.: Condens. Matter **20** (2008) 155208 (8pp) doi:10.1088/0953-8984/20/15/155208

Anisotropic magnetoresistance in Fe/MgO/Fe tunnel junctions

M N Khan[1], J Henk[2] and P Bruno[2,3]

[1] Indian Institute of Technology (IIT) Kharagpur, Kharagpur 721302, India
[2] Max-Planck-Institut für Mikrostrukturphysik, Weinberg 2, D-06120 Halle (Saale), Germany

E-mail: henk@mpi-halle.de

Received 17 December 2007, in final form 26 February 2008
Published 25 March 2008
Online at stacks.iop.org/JPhysCM/20/155208

Abstract
The ballistic conductance of Fe/MgO/Fe magnetic tunnel junctions depends significantly on the direction of the magnetization in the leads, as is investigated by relativistic first-principles electronic structure and transport calculations. The rotation of the parallel aligned lead magnetizations from in-plane to perpendicular orientation with respect to the interfaces, that is tunnel anisotropic magnetoresistance (TAMR), increases the zero-bias conductance by about 30%. The effect originates from both the Rashba spin–orbit interaction at the interfaces and from resonant tunneling. Spin–orbit induced band gaps in the leads show no considerable effect on the anisotropic magnetoresistance. The tunnel magnetoresistance (TMR), i.e. the dependence of the conductance on the mutual angle between the lead magnetizations, is also addressed.

(Some figures in this article are in colour only in the electronic version)

1. Introduction

The transport properties of a magnetoelectronic device are typically changed by an external magnetic field [1, 2]. For example, in magnetic tunnel junctions the magnetizations in the two ferromagnetic leads can be aligned either parallel (P) or antiparallel (AP) to each other, depending on the strength and sign of the applied field. Correspondingly, the resistances ρ(P) and ρ(AP) differ (e.g. [3–7]), as is commonly expressed by the magnetoresistance ratio. The latter is defined as the relative change of ρ(AP) with respect to ρ(P). This effect is named tunnel magnetoresistance (TMR; e.g. [8]), similar to the giant magnetoresistance for a spin-valve structure (e.g. [9]).

The resistivity of bulk ferromagnetic samples also depends on the direction of an external magnetic field [10]. This anisotropic magnetoresistance (AMR) was discovered 1857 by Thomson [11]. Since the transport in extended samples is diffusive, the effect is attributed to electron–electron scattering and to scattering at defects, in particular to sd impurity scattering [12, 13]. The angular dependence of the resistivity is given by

$$\rho(\theta) = \rho_\perp + (\rho_\parallel - \rho_\perp)\cos^2\theta, \qquad (1)$$

where $\rho_\parallel$ ($\rho_\perp$) is the resistivity with the external field along (perpendicular to) the direction of the electric current. θ is the angle between magnetic field and current. Typically one finds $\rho_\parallel < \rho_\perp$, with a difference of the order of 5%. The angular dependence is necessarily a spin–orbit effect because the spin–orbit interaction is the only mechanism which couples the electronic spin degrees of freedom (which are affected by the magnetic field) to the orbital degrees of freedom (which determine the charge transport).

In contrast to diffusive transport in bulk samples, transport in nanostructures may be ballistic. The ballistic anisotropic magnetoresistance (BAMR) is observed in ferromagnetic nanocontacts, e.g. in nanowires [14] (for conductance oscillations with wire length see [15]). The anisotropic conductance changes abruptly upon variation of θ, in contrast to the continuous behavior of the AMR, equation (1). Due to the spin–orbit interaction, the number of bands which cross the Fermi level depends on θ [16]. Therefore, the number $N(\theta)$ of scattering channels which contribute to the conductance changes likewise, and the conductance displays consequently a step-wise dependence on θ. Since the number of channels in an ultrathin nanowire is small, the BAMR ratio $[N(\theta) - N(0)]/N(0)$ is of the order of a few tens per cent.

Another type of nanodevices which show anisotropic magnetoresistance is magnetic tunnel junctions. The tunnel anisotropic magnetoresistance (TAMR) is found in junctions

[3] Present address: European Synchrotron Radiation Facility–BP 220, F-38043 Grenoble Cedex, France.

which comprise at least one ferromagnetic electrode, e.g. a ferromagnetic (FM) and a nonmagnetic (NM) electrode separated by an insulating spacer (I) [17, 18]. Origins of the TAMR to come into question are (i) spin–orbit induced gaps in the band structure of the FM electrode, (ii) the Rashba effect [19] at the FM/I interface, and (iii) resonant states whose coupling to the scattering channels depends on the magnetization direction. The prospects of TAMR devices are that they may maintain ballistic transport and are easier to produce than nanocontacts (e.g. break junctions).

The number of channels which contribute essentially to the tunnel conductance of a planar magnetic junction is typically much smaller than the total number of channels. In other words, tunneling filters out a significant part of the phase space (i.e. the two-dimensional Brillouin zone). By geometric constraints—as in a nanowire—the number of channels can be further reduced, resulting in an increased magnetoresistance [20] (for AMR and TAMR in break junctions and nanoconstrictions see [21, 22]).

The spin–orbit interaction affects the electronic structure of a junction, and thus its conductance, in two ways. First, it leads to gaps in the band structure of the electrodes. The latter would reduce the number of available conducting channels. Second, the Rashba effect can lift degeneracies in the electronic structure at the interfaces. Note that effects due to spin–orbit coupling are typically stronger at an interface than in the bulk, due to the potential gradient at the interface [23].

A large TAMR ratio is expected if (i) there are spin-polarized interface resonances [24, 25], (ii) the interfaces produce a large Rashba effect, e.g. by a large potential gradient, and (iii) if the nonmagnetic electrode shows a featureless transmission close to the Fermi energy (e.g. Cu with its free-electron-like sp band). TAMR ratios of up to 20% are theoretically predicted for custom-tailored Fe(001)/vacuum/bcc-Cu(001) tunnel junctions [17].

Magnetic tunnel junctions usually comprise two ferromagnetic electrodes separated by an oxide spacer (FM/I/FM; e.g. [26, 27]), rather than being separated by a vacuum barrier. While a junction with a vacuum barrier and a Cu electrode is not very selective in phase space, a question arises whether a considerable TAMR ratio can be maintained in a highly phase-space selective FM/I/FM junction [28–32]. Phase-space selection is found for example in Fe/MgO/Fe junctions (e.g. [33]).

From the above it is evident that there is need for an *ab initio* investigation of the anisotropic conductance in magnetic tunnel junctions with two ferromagnetic electrodes. In this paper we present and discuss results of first-principles electronic structure and transport calculations of the TAMR in Fe/FeO/MgO/FeO/Fe junctions. The ballistic transport is calculated according to Landauer–Büttiker theory [34], as implemented in relativistic multiple-scattering theory (layer Korringa–Kohn–Rostoker method). For symmetric junctions (i.e. a FeO layer at both interfaces) the conductance is significantly influenced by resonant tunneling, leading to so-called hot spots in the transmittance maps [35–37]. In contrast to an FM/I/NM junction, we are concerned with two magnetic electrodes (FM/I/FM) which allows us to study both the tunnel magnetoresistance (TMR) and the tunnel anisotropic magnetoresistance (TAMR). To investigate TMR, the magnetization orientation of one of the leads is kept fixed while that in the other lead is rotated. For the TAMR, the lead magnetizations are parallel aligned but their angle with respect to the crystal axes is varied. Please note that the effect of spin–orbit coupling on the spin-dependent transport was studied by Li and Chang by means of a tight-binding model [38].

The paper is outlined as follows. Details of the computations are provided in section 2. The effect of bulk-band gaps which are induced by spin–orbit coupling on the conductance is addressed for Fe electrodes in section 3. The TMR and the TAMR in a Fe/FeO/MgO/FeO/Fe tunnel junction are discussed in section 4, focusing here on the Rashba effect and on resonant tunneling.

2. Computational

The ballistic transport calculations are based on first-principles electronic structure calculations for Fe/MgO/Fe magnetic tunnel junctions, as reported in [35]. The local spin-density approximation to density functional theory with the Perdew–Wang exchange–correlation functional is applied [39]. In the present paper we focus on symmetric junctions with four MgO layers as spacer. MgO spacer and Fe electrodes are separated by FeO layers at both interfaces (i.e. an Fe(001)/FeO/$(MgO)_4$/FeO/Fe(001) junction). The relaxed interface geometry is taken from x-ray diffraction experiments [35]. In contrast to that experiment [35], which finds partially occupied oxygen sites in the FeO layer, fully occupied FeO layers are assumed.

The transport calculations are performed with the spin-polarized relativistic layer Korringa–Kohn–Rostoker computer code OMNI2K [40, 41] which involves solving the Dirac equation for magnetic sites [42]. The ballistic conductance C for a planar tunnel junction is calculated within the Landauer–Büttiker approach [34],

$$C = \frac{e^2}{h} \int_{2\mathrm{BZ}} T(E_\mathrm{F}; \boldsymbol{k}_\parallel)\, \mathrm{d}k_\parallel^2. \tag{2}$$

C is computed within a scheme proposed by MacLaren *et al* [43]. For zero-bias voltage the energy is restricted to the Fermi energy E_F. Transport is along the z-axis, i.e. perpendicular to the layers.

The transmittance $T(E_\mathrm{F}; \boldsymbol{k}_\parallel)$ is integrated over the two-dimensional Brillouin zone (2BZ), by using more than 40 000 wavevectors. It comprises a sum over all pairs of Bloch states (i.e. the scattering channels) with energy E and wavevector $\boldsymbol{k}_\parallel = (k_x, k_y)$ which are incoming in one electrode and outgoing in the other electrode,

$$T(E; \boldsymbol{k}_\parallel) = \sum_{nm} T_{n\to m}(E; \boldsymbol{k}_\parallel). \tag{3}$$

$T_{n\to m}(E; \boldsymbol{k}_\parallel)$ is the probability for transmission of the incoming Bloch state with band index n through the spacer into the outgoing Bloch state with band index m. A convenient tool for analyzing details of the transport are transmittance maps which display $T(E; \boldsymbol{k}_\parallel)$ versus $\boldsymbol{k}_\parallel$ at energy E.

Since interfaces determine considerably the transport properties (e.g. [44–48]), transmittance maps need to be interpreted by means of the local electronic structure, rather than by the electronic structures of the bulk electrodes. The former is obtained from the spectral density

$$N_{la}(E;\boldsymbol{k}_\parallel) = -\frac{1}{\pi}\,\mathrm{Im}\,\mathrm{Tr}\,G^{+}_{la,la}(E;\boldsymbol{k}_\parallel) \tag{4}$$

of atom a in layer l. $G^{+}_{la,la}$ is the site-diagonal Green function of that site. The trace involves integration over the muffin-tin sphere and summation over spin angular quantum numbers [42]. Spectral density maps display $N_{la}(E;\boldsymbol{k}_\parallel)$ versus $\boldsymbol{k}_\parallel$ for both energy and site fixed, similar to transmittance maps.

The tunnel magnetoresistance (TMR) is defined as the variation of the tunnel conductance C of the junction upon changing the mutual angle θ of the magnetization directions $\boldsymbol{M}_\mathcal{L}$ and $\boldsymbol{M}_\mathcal{R}$ of the electrodes. Here, $\mathcal{L}$ ($\mathcal{R}$) indicates the 'left' ('right') electrode. Due to spin–orbit coupling, the conductance depends on the direction of the magnetizations with respect to a crystal axis. For investigating TMR we keep $\boldsymbol{M}_\mathcal{R}$ parallel to the $[hkl]$ direction (here [001] or [100]) while rotating $\boldsymbol{M}_\mathcal{L}$ in a given plane (here in the (010) plane). For $\boldsymbol{M}_\mathcal{R}$ parallel to [001] and [100], $\boldsymbol{M}_\mathcal{L} = (\sin\theta, 0, \cos\theta)$ and $\boldsymbol{M}_\mathcal{L} = (\cos\theta, 0, \sin\theta)$, respectively. The 'optimistic' TMR ratio is then given by

$$\delta_{[hkl]} \equiv \frac{C(\mathrm{P}) - C(\mathrm{AP})}{C(\mathrm{AP})} = \frac{C(0°) - C(180°)}{C(180°)}, \tag{5}$$

i.e. the conductance change from parallel (P) to antiparallel (AP) alignment. The subscript $[hkl]$ indicates the direction of $\boldsymbol{M}_\mathcal{R}$.

Without spin–orbit coupling, the angular dependence of the conductance is given by $C(\theta) \propto a + b\cos\theta$, as was shown for free electrons by Slonczewski [49]. It appears as a pure spin effect, namely due to rotation of spin quantization axes [50, 51]. If spin–orbit coupling is taken into account, the spin degrees of freedom are coupled to the orbital degrees of freedom and, as a result, the angular dependence is expected to differ from the cos-behaviour [52].

The tunnel anisotropic magnetoresistance (TAMR) is the change of the conductance for parallel lead magnetizations upon rotating these in a given crystal plane (here, the (010) plane). With θ being the angle with respect to the [001] direction ($\boldsymbol{M}_\mathcal{L} = \boldsymbol{M}_\mathcal{R} = (\sin\theta, 0, \cos\theta)$), we define the TAMR ratio as

$$\Delta \equiv \frac{C([001]) - C([100])}{C([100])} = \frac{C(0°) - C(90°)}{C(90°)}, \tag{6}$$

in accordance with [17].

3. Ballistic anisotropic magnetoresistance of Fe(001)

As a prequel, the ballistic anisotropic magnetoresistance is addressed in order to establish both the signature of bulk-band gaps in transmittance maps and the importance of phase-space filtering. For this purpose we choose as a 'toy model' an Fe(001) electrode, in analogy to an infinitely long nanowire which shows BAMR [16]. The transmittance is computed in an $(E;\boldsymbol{k}_\parallel)$-region in which a spin–orbit induced band gap shows up dependent on the magnetization direction.

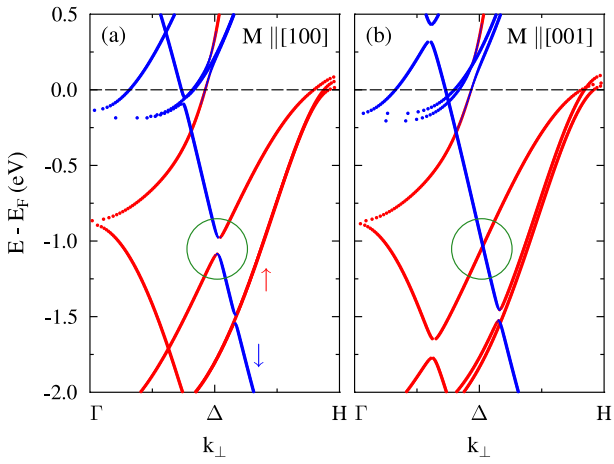

Figure 1. Spin-resolved relativistic band structure of Fe of the Γ–Δ–H line (along [001]) for magnetization $\boldsymbol{M} \parallel [100]$ (a) and $\boldsymbol{M} \parallel [001]$ (b). The spin orientation is color coded as red (medium grey) and blue (dark grey) for spin up (↑) and down (↓), respectively. Circles highlight the spin–orbit induced band gap at $E = -1.05$ eV, being present for $\boldsymbol{M} \parallel [100]$ (a) but closed for $\boldsymbol{M} \parallel [001]$ (b).

The Fe band structure of the Γ–Δ–H line along [001] ($\boldsymbol{k}_\parallel = \boldsymbol{0}$; figure 1) exhibits several band gaps induced by spin–orbit coupling, in dependence on the magnetization direction [53]. We concentrate on the gap at $E = -1.05$ eV and $k_\perp \approx 0.5|\Gamma\text{–}\Delta\text{–}\mathrm{H}|$, which shows up for the magnetization $\boldsymbol{M} \parallel [100]$ (indicated by a circle in figure 1(a)). The gap is closed for $\boldsymbol{M} \parallel [001]$ (figure 1(b)). In the spectral density map for $E = -1.05$ eV the band gap appears as a sharp, circular minimum with a radius of 0.04 Bohr^{-1} for $\boldsymbol{M} \parallel [100]$ (figure 2(a)). In contrast, the spectral density is smooth for $\boldsymbol{M} \parallel [001]$ (figure 2(b)).

Ballistic transport in an ideal electrode is discussed in terms of the Sharvin conductance [54]. Because the Bloch states are not scattered one finds $T_{n\to m}(E;\boldsymbol{k}_\parallel) = \delta_{nm}$, and the transmittance $T(E;\boldsymbol{k}_\parallel)$ equals the number of Bloch states which propagate in the [001] direction at $(E;\boldsymbol{k}_\parallel)$. The number of these Bloch states is three at the band gap (figure 1(a); $\boldsymbol{M} \parallel [100]$), as is the transmittance in the center of the 2BZ (figure 2(c)). The gap is closed for $\boldsymbol{M} \parallel [001]$ and the transmittance is increased to five (figures 1(b) and 2(d)).

In these model calculations a band gap is easily identified as a rather extended minimum in both the spectral density and the transmittance maps. To address its effect on the conductance, the transmittance is integrated in the central part of the 2BZ. For the Fe leads magnetized along [100] and [001] one obtains 4.792 and 4.841 for the total transmittance, respectively, which is a relative change of about 1.02%. The change in the spectral densities is even less (58.034 states Harteee^{-1} for $\boldsymbol{M} \parallel [100]$ compared to 58.328 states Hartree^{-1} for $\boldsymbol{M} \parallel [001]$, that is about 0.50%). Hence one is led to conclude that band gaps in

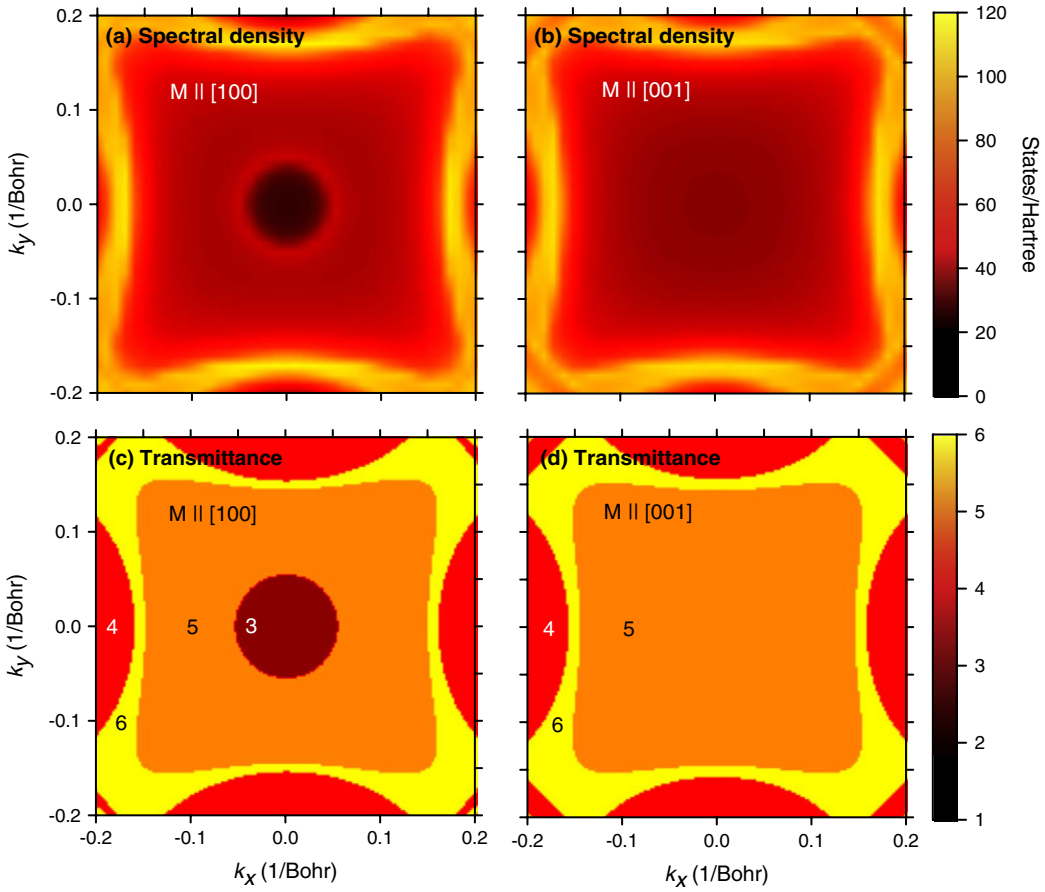

Figure 2. Spectral density (top row, (a) and (b)) and transmittance (bottom row, (c) and (d)) of Fe(001) for $E = -1.05$ eV at the center of the 2BZ, depicted as color scales (grey scales). The magnetization M is parallel to [100] (left column, (a) and (c)) and [001] (right column, (b) and (d)). The k_x-axis (k_y-axis) is along [100] ([010]). The number of Bloch states which propagate in the [001] direction is indicated in (c) and (d). The band gap marked in figure 1 appears as a circular minimum about $(k_x, k_y) = \mathbf{0}$ for $M \parallel [100]$ ((a) and (c)).

the electrodes produce no significant effect in the current–voltage characteristics of a planar tunnel junction. In contrast, the sizable BAMR of a narrow nanocontact can be attributed to the lateral constriction which reduces the phase space. Considering only $\boldsymbol{k}_\parallel = \mathbf{0}$, the BAMR for the Fe electrode would be $(5-3)/3$ or 67%. Hence, phase space filtering—as is typically present in realistic tunnel junctions—could provide a means for obtaining a significant TAMR ratio.

Summarizing so far, we find that spin–orbit induced band gaps in the electrodes show up as extended minima in the transmittance maps (figure 2). Their effect is however comparably small if the total number of conduction channels is large. This finding suggests that phase space filtering is essential for achieving a large TAMR.

4. Anisotropic magnetoresistance of Fe/MgO/Fe tunnel junctions

Having ruled out bulk-band gaps as a source for a large TAMR, we now turn to the Rashba effect and resonant tunneling. A signature of the Rashba effect (e.g. [19, 23, 55]) at a magnetic surface is a spin-dependent shift of features in the spectral density maps, most prominently for surface states. The displacement is perpendicular to the in-plane magnetization, as was demonstrated for Gd(0001) [56]. The effect also shows up for surface resonances in Fe(001) and manifests itself in an anisotropic conductance [17, 52].

The strength of the Rashba effect depends on both the atomic number and on the potential gradient at the interface [57, 58]. For an Fe(001) surface the latter is mainly attributed to the slope of the vacuum barrier. At an Fe/FeO/MgO interface, however, the potential gradient may be significantly smaller. Consequently, the Rashba effect might be too small to produce a sizable TAMR ratio.

An interface resonance is an electronic state which is resonant with Bloch states of the lead and shows an increased probability density at the interface. A 'handshake' of two resonances located at either interface of a planar junction can increase the transmittance considerably. A signature of such resonant tunneling is a transmittance close to unity (i.e. orders of magnitude larger than in the rest of the 2BZ). Consequently, resonant tunneling may essentially govern the conductance [24, 59–61] although it shows up in tiny parts of the 2BZ, in so-called 'hot spots'. Both interface resonances have to appear necessarily at the same $(E; \boldsymbol{k}_\parallel)$. In symmetric tunnel junctions a 'handshake' is more likely than in asymmetric junctions. Note that the symmetry of real samples is typically broken, due to an inherent structural asymmetry

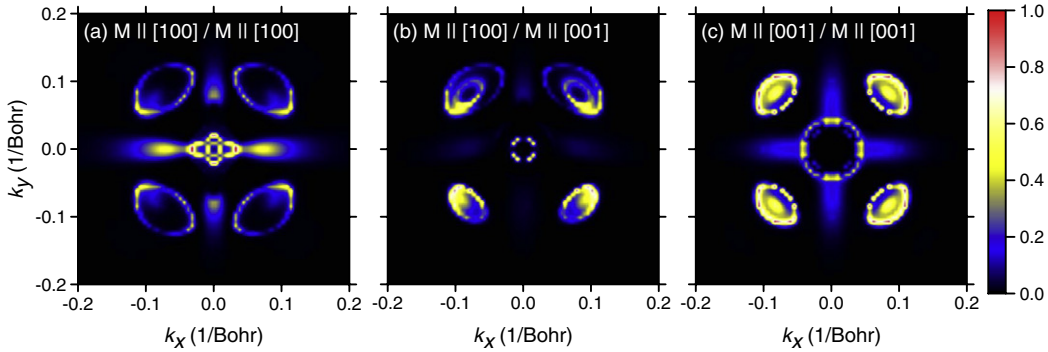

Figure 3. Zero-bias transmittance maps of Fe/FeO/$(MgO)_4$/FeO/Fe tunnel junctions for different magnetic configurations: magnetizations along [100] in both leads (a), along [100] in one lead and along [001] in the other lead (b), and along [001] in both leads (c), depicted as a color scale (grey scale) in the central part of the 2BZ.

(e.g. Fe/FeO/MgO/Fe or Fe/vacuum/Cu), to disorder or to a nonzero bias voltage. The 'handshake' may therefore by less likely in these systems [36].

The magnetization direction in the electrodes affects via spin–orbit coupling both the Bloch states and the interface resonances, and hence their coupling [17]. If the magnetizations in the electrodes are parallel, resonant tunneling is preferred. The symmetry is however broken by a nonzero mutual angle θ between the magnetizations (i.e. TMR). And as a result, the transmittance is reduced in the hot spots. If the magnetizations in both leads are rotated simultaneously (i.e. TAMR), for example from the [001] into the [100] direction, the electronic structure at the interfaces is changed by the Rashba effect and, thus, the conductance is changed as well. This effect can be visualized as deformations in transmittance maps and in the associated spectral density maps.

To investigate the aforementioned effects in perspicuity we focus on symmetric tunnel junctions and zero-bias voltage, that is a case where the anisotropic magnetoresistance due to resonant tunneling should be considerable. To strengthen the discussion further it is concentrated on transmittance and spectral density maps of the central part of the 2BZ (note that for thick spacers mostly channels with small $|\boldsymbol{k}_\parallel|$ contribute to the conductance).

The transmittance map for the junction with both lead magnetizations $\boldsymbol{M}_\mathcal{L}$ and $\boldsymbol{M}_\mathcal{R}$ parallel to [100] shows a twofold rotational symmetry (point group $2mm$; figure 3(a)). The transmittance is large in four ring-like features at about $(k_x, k_y) = (\pm 0.08, \pm 0.08)$ Bohr^{-1}. These appear due to resonant tunneling, as is evident from the transmittance being very close to unity. There is also resonant tunneling at the center of the 2BZ and at the bar-shaped features at $k_y = 0$. As anticipated, one finds a strong filtering of the phase space due to resonant tunneling, that is the transmittance is sizable solely in small parts of the 2BZ.

Rotating $\boldsymbol{M}_\mathcal{R}$ towards [001] while keeping $\boldsymbol{M}_\mathcal{L}$ along [100] (figure 3(b)), a central ring of large transmittance with small radius appears. The bar-shaped features have completely disappeared, implying that resonant tunneling is suppressed in this $(E; \boldsymbol{k}_\parallel)$-region. Also striking is the deformation of the four ring-like structures, a characteristic of the Rashba effect [56]. Note further that the twofold rotational symmetry of the transmittance map is reduced to a reflection symmetry about the k_y axis (point group m). The difference between figures 3(a) and (b) is a signature of TMR because the angle θ between the magnetizations is nonzero in figure 3(b), as opposed to figure 3(a).

The map for the junction with both lead magnetizations parallel to [001] shows a fourfold rotational symmetry (point group $4mm$; figure 3(c)). The transmittance is clearly largest in the four ring-like features. The associated spectral density reveals a 'handshake' of interface resonances which comprise mostly spin-down sp orbitals at the oxygen sites in the MgO spacer (not shown). Note also the central ring of large transmittance with a radius of 0.04 Bohr^{-1}, which is a significantly larger radius than that in figure 3(b). The difference between figures 3(a) and (c) indicates TAMR because the angle of the parallel lead magnetizations with respect to a crystal axis is changed.

To explain prominent features in the transmittance maps, we present in figure 4 spectral density maps at selected sites for a lead magnetization $\boldsymbol{M}$ along [100] (left column) and [001] (right column), respectively. Note that there is no strict one-to-one correspondence of transmittance and spectral density. Features in the transmittance maps are nevertheless expected to have counterparts in the spectral density maps (e.g. [48]).

Already in the Fe bulk layers (first row in figure 4) one finds a significant spin–orbit induced deformation of the spectral density. In particular for $\boldsymbol{M} \parallel [001]$ (figure 4(b)), the bright central ring shows up as in the transmittance (figure 3(c)).

A Rashba deformation appears in the FeO layer (second row in figure 4). The two arcs with $k_y > 0$ (figure 4(d)) are shifted to larger k_y values (figure 4(c)). The spectral density of those with $k_y < 0$ (figure 4(d)) is reduced in figure 4(c). In the transmittance maps this effect shows up as increased radii of the four ring-like structures (compare figures 3(c) with (a) and (b)).

Also the oxygen site of the first MgO layers (adjacent to the FeO layer) displays a profound effect (third row in figure 4). The cross-like feature in figure 4(f) is almost reduced to a spot

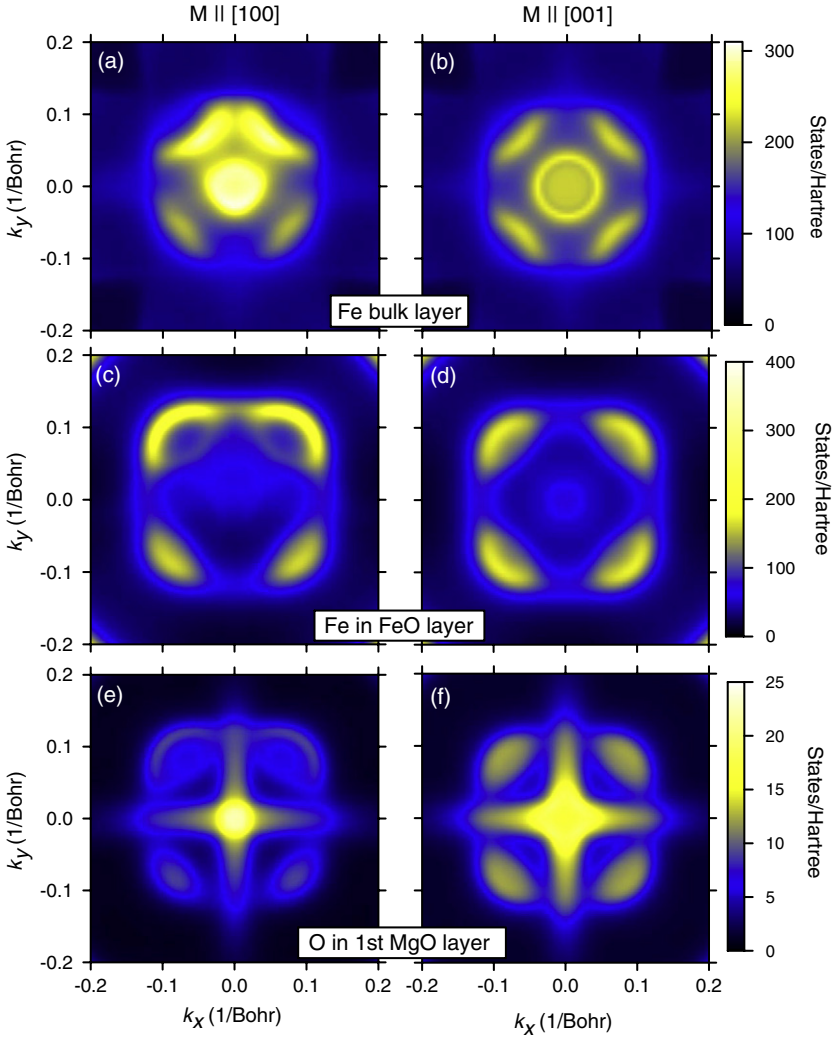

Figure 4. Atom-resolved spectral densities of an Fe/FeO/$(MgO)_4$/FeO/Fe tunnel junction for two different magnetic configurations: magnetization along [100] (left column) and along [001] (right column) at the Fermi energy. The selected sites are Fe bulk ((a) and (b)), Fe in the FeO interface layer ((c) and (d)), and O in the first MgO spacer layer ((e) and (f)). The color scales (grey scales) vary from row to row. Only the central part of the 2BZ is displayed.

in figure 4(e). The four bright arcs in figure 4(f) show up as sizable transmittance in figure 3(c). These do not appear in figure 4(e) and thus appear with a reduced transmittance in figure 3(b). The transmittance is even more reduced in figure 3(a).

For the junction with both $\boldsymbol{M}_{\mathcal{L}}$ and $\boldsymbol{M}_{\mathcal{R}}$ parallel to [100] resonant tunneling is mainly mediated by oxygen $p_y p_z$ orbitals, whereas for the [001] direction mostly oxygen $p_x p_y$ orbitals contribute, as is found by investigating the spectral density at selected hot spots.

The analysis of the spectral density maps corroborates the explanation of the anisotropic transmittances by the Rashba effect in interplay with resonant tunneling. The main signatures are strongly confined areas in the 2BZ with large spectral weight and a magnetization-dependent reduction of the symmetry of the maps. For $\boldsymbol{M} \parallel [001]$ the point group is $4mm$, which is reduced to m for $\boldsymbol{M} \parallel [100]$ (reflection about the k_y axis, i.e. perpendicular to $\boldsymbol{M}$).

For Fe(001)/vacuum/bcc-Cu(001) junctions it is found that the spin-flip transmission for $\boldsymbol{M} \parallel [001]$ is less than for $\boldsymbol{M} \parallel [100]$ [17]. This finding was explained by the intrinsic broadening of interface resonances which is influenced by spin–orbit coupling. By analyzing the Bloch state resolved transmittance $T_{n\to m}(E; \boldsymbol{k}_\parallel)$ at selected hot spots, we find the same behavior in the Fe/MgO/Fe junction, thus corroborating the explanation by Chantis *et al* [17].

Having addressed qualitatively the effect of spin–orbit coupling on the transmittance, we discuss now the TMR for the magnetizations along [001] and [100]. For $\boldsymbol{M}_{\mathcal{R}} \parallel [001]$, the conductances for the parallel (P, $\theta = 0°$) and the antiparallel (AP, $\theta = 180°$) configurations are $C_{[001]}(\mathrm{P}) = 0.01116\ e^2/h$ (figure 3(c)) and $C_{[001]}(\mathrm{AP}) = 0.000\,26\ e^2/h$, respectively. For $\boldsymbol{M}_{\mathcal{R}} \parallel [100]$, we find $C_{[100]}(\mathrm{P}) = 0.007\,73\ e^2/h$ (figure 3(a)) and $C_{[100]}(\mathrm{AP}) = 0.000\,25\ e^2/h$. The TMR ratios, as defined in equation (5), are $\delta_{[001]} = 4205\%$ and $\delta_{[100]} = 2956\%$, indicating a sizable change with respect to the magnetization direction $[hkl]$.

The conductance $C_{[100]}(\mathrm{P})$ is significantly reduced (by 31%) with respect to $C_{[001]}(\mathrm{P})$, as is evident by visual

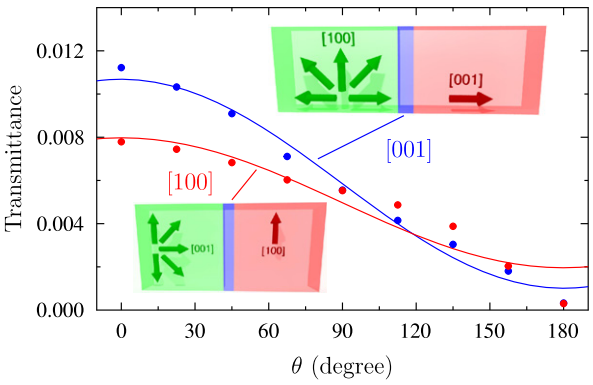

Figure 5. Zero-bias transmittances of Fe/FeO/(MgO) $_4$ /FeO/Fe tunnel junctions versus angle θ between the magnetizations $\boldsymbol{M}_{\mathcal{L}}$ and $\boldsymbol{M}_{\mathcal{R}}$ of the Fe leads (i.e. TMR). In the case '[001]' (blue (dark grey) symbols) $\boldsymbol{M}_{\mathcal{R}}$ is parallel to [001], while for '[100]' (red (medium grey) symbols) $\boldsymbol{M}_{\mathcal{R}}$ is parallel to [100]. $\boldsymbol{M}_{\mathcal{L}}$ is rotated in the (010) plane (see insets for schematic representations of the MTJ). The magnetizations are parallel for $\theta = 0°$, orthogonal for $\theta = 90°$, and antiparallel for $\theta = 180°$ (the symbols at 180° overlap). cos-fits to the data are given by solid lines.

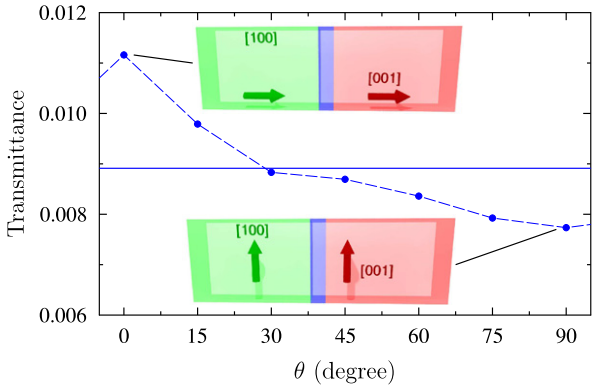

Figure 6. Zero-bias transmittances of Fe/FeO/(MgO) $_4$ /FeO/Fe tunnel junctions versus angle θ between the parallel magnetizations of the Fe leads and the [001] direction (i.e. TAMR). The magnetizations are along [001] ([100]) for $\theta = 0°$ ($\theta = 90°$). A dashed line serves as guide to the eye. A constant (solid line) is fitted to the data.

comparison of figure 3(a) with (c). The TAMR ratio Δ defined in equation (6) is 44%. In contrast, the respective AP conductance is reduced by only 2%. Please note that the difference in the P conductances is of the same order as found theoretically for Fe/vacuum/Cu junctions [17].

For investigating the dependence of the conductance on the mutual magnetization angle θ, $\boldsymbol{M}_{\mathcal{R}}$ was fixed—parallel to [001] and [100]—while $\boldsymbol{M}_{\mathcal{L}}$ was rotated in the [010] plane (cf section 2). In other words, we are addressing the evolution of the conductance from the P to the AP alignment, that is TMR. The transmittances of both configurations follow approximately the cos dependence which would have been obtained without spin–orbit coupling (cf. the $a + b\cos\theta$ fit to the data) [49]. Hence, the deviations from this behavior are attributed to the spin–orbit interaction. Note that both curves coincide for $\theta = 90°$, due to symmetry. Further, the data points overlap at $\theta = 180°$.

A significant deviation from the cos dependence was recently found in MTJs with CoFe leads and MgO as well as Al_2O_3 spacers [52]. The higher-order contribution was attributed to an interface resonance that affects the transmittance of the contributing scattering channels by the spin–orbit interaction, as revealed by tight-binding calculations. This observation is in agreement with the present findings of a significant higher-order contribution to angular dependence (i.e. a $\cos(2\theta)$ term).

As is evident from figure 5, the transmittance depends on the direction of the parallel electrode magnetizations (compare the cases '[100]' and '[001]' for $\theta = 0°$), that is TAMR. The dependence on the angle with respect to the [001] direction is given in figure 6, with the magnetizations rotated within the (010) plane. Due to symmetry, which gives $C(\theta) = C(-\theta)$ and $C(90° + \theta) = C(90° - \theta)$, it is sufficient to display the θ-range from 0° to 90°. The transmittance (symbols) follows roughly a $\cos(2\theta)$ dependence but with significant deviations. Note that without spin–orbit coupling the transmittance would not depend on θ at all, as is visualized by a constant fitted to the data (solid line in figure 6). Hence, spin–orbit coupling has a significant effect on the conductance of magnetic tunnel junctions.

In conclusion, the Rashba effect in co-action with resonant tunneling provides an efficient mechanism for anisotropic magnetoresistance in symmetric tunnel junctions. Essential ingredients are a strong reduction of the phase space which contributes sizably to the conductance ('hot spots') and a significant deformation of the spectral density by spin–orbit coupling.

5. Concluding remarks

Our theoretical analysis supports that the Rashba effect in interplay with a reduction of phase space serves as a mechanism for the tunneling anisotropic magnetoresistance (TAMR) in planar junctions with two ferromagnetic leads. The Rashba effect changes the spin-dependent electronic structure at the ferromagnet/spacer interfaces, in dependence on the direction of the external magnetic field. Moreover, the phase space is reduced for example by interface resonances with a large transmission probability. This opens the possibility to utilize the magnetic field direction as a means to change the conductance of a magnetoelectronic device, in addition to the conventional field reversal.

Investigated by relativistic first-principles calculations for idealized tunnel junctions the TAMR is sizable, but it might be less in realistic systems. In particular, resonant tunneling may be reduced by imperfections at the interfaces. To estimate the size of the reduction, transport calculations including disorder and for nonzero bias voltage need to be performed, preferably in conjunction with experiments.

References

[1] Hartmann U (ed) 1999 *Magnetic Multilayers and Giant Magnetoresistance. Fundamentals and Industrial Applications* (*Springer Series in Surface Sciences* vol 37) (Berlin: Springer)

[2] Prinz G A 2005 *Ultrathin Magnetic Structures IV. Applications of Nanomagnetism* ed B Heinrich and J A C Bland (Berlin: Springer) chapter 2 p 5
[3] Daughton J M 1999 *J. Magn. Magn. Mater.* **192** 334
[4] Grünberg P 2001 *J. Phys.: Condens. Matter* **13** 7691
[5] Tsymbal E Y and Pettifor D G 2001 *Solid State Physics* vol 56, ed H Ehrenreich and F Spaepen (San Diego, CA: Academic) p 113
[6] Klemmer T J, Sun J Z, Fert A and Bass J (ed) 2002 *Spintronics* (*Symp. Proc.* vol 260) (Warrendale: Materials Research Society)
[7] Žutić I, Fabian J and Das Sarma S 2004 *Rev. Mod. Phys.* **76** 323
[8] LeClair P, Moodera J S and Swagten H J M 2005 *Ultrathin Magnetic Structures III. Fundamentals of Nanomagnetism* ed J A C Bland and B Heinrich (Berlin: Springer) chapter 3 p 51
[9] Barthélémy A, Fert A and Petroff F 1999 *Handbook of Magnetic Materials* vol 12, ed K H J Buschow (Amsterdam: Elsevier) p 1
[10] Ebert H, Banhart J and Vernes A 2001 *Encyclopedia of Materials: Science and Technology* ed K H J Buschow (Amsterdam: Elsevier) p 5079
[11] Thomson W 1857 *Proc. R. Soc.* **8** 546
[12] Potter R I 1974 *Phys. Rev.* B **10** 4626
[13] McGuire T R and Potter R I 1975 *IEEE Trans. Magn.* **11** 1018
[14] Sokolov A, Zhang C, Tsymbal E Y, Redepenning J and Doudin B 2007 *Nat. Nanotechnol.* **2** 171
[15] Czerner M, Bagrets A, Stepanyuk V S, Klavsyuk A L and Mertig I 2006 *Phys. Rev.* B **74** 115108
[16] Velev J, Sabirianov R F, Jaswal S S and Tsymbal E Y 2005 *Phys. Rev. Lett.* **94** 127203
[17] Chantis A N, Belashchenko K D, Tsymbal E Y and van Schilfgaarde M 2007 *Phys. Rev. Lett.* **98** 046601
[18] Moser J, Matos-Abiague A, Schuh D, Wegscheider W, Fabian J and Weiss D 2007 *Phys. Rev. Lett.* **99** 056601
[19] Bychkov Y A and Rashba E I 1984 *J. Phys. C: Solid State Phys.* **17** 6039
[20] Moodera J S, Kinder L R, Nowak J, LeClair P and Meservey R 1996 *Appl. Phys. Lett.* **69** 708
[21] Giddings A D, Khalid M N, Jungwirth T, Wunderlich J, Yasin S, Campion R P, Edmonds K W, Sinova J, Ito K, Wang K Y, Williams D, Gallagher B L and Foxon C T 2005 *Phys. Rev. Lett.* **94** 127202
[22] Bolotin K I, Kuemmeth F and Ralph D C 2006 *Phys. Rev. Lett.* **97** 127202
[23] Winkler R 2003 *Spin–Orbit Coupling Effects in Two-Dimensional Electron and Hole Systems* (Berlin: Springer)
[24] Dederichs P H, Mavropoulos P, Wunnicke O, Papanikolaou N, Bellini V, Zeller R, Drchal V and Kudrnovský J 2002 *J. Magn. Magn. Mater.* **240** 108
[25] Tiusan C, Faure-Vincent J, Bellouard C, Hehn M, Jougoulet E and Schuhl A 2004 *Phys. Rev. Lett.* **93** 106602
[26] Faure-Vincent J, Tiusan C, Jouguelet E, Canet F, Sajieddine M, Bellouard C, Popova E, Hehn M, Montaigne F and Schuhl A 2003 *Appl. Phys. Lett.* **82** 4507
[27] Yuasa S, Nagahama T, Fukushima A, Suzuki Y and Ando K 2004 *Nat. Mater.* **3** 868
[28] Brey L, Tejedor C and Fernández-Rossier J 2004 *Appl. Phys. Lett.* **85** 1996
[29] Gould C, Rüster C, Jungwirth T, Girgis E, Schott G M, Giraud R, Brunner K, Schmidt G and Molenkamp L W 2004 *Phys. Rev. Lett.* **93** 117203
[30] Rüster C, Gould C, Jungwirth T, Sinova J, Schott G M, Giraud R, Brunner K, Schmidt G and Molenkamp L W 2005 *Phys. Rev. Lett.* **94** 027203
[31] Saito H, Yuasa S and Ando K 2005 *Phys. Rev. Lett.* **95** 086604
[32] Sankowski P, Kacman P, Majewski J A and Dietl T 2007 *Phys. Rev.* B **75** 045306
[33] Mathon J and Umerski A 2001 *Phys. Rev.* B **63** 220403(R)
[34] Imry Y and Landauer R 1999 *Rev. Mod. Phys.* **71** S306
[35] Tusche C, Meyerheim H L, Jedrecy N, Renaud G, Ernst A, Henk J, Bruno P and Kirschner J 2005 *Phys. Rev. Lett.* **95** 176101
[36] Velev J P, Belashchenko K D and Tsymbal E Y 2006 *Phys. Rev. Lett.* **96** 119601
[37] Tusche C, Meyerheim H L, Jedrecy N, Renaud G, Ernst A, Henk J, Bruno P and Kirschner J 2006 *Phys. Rev. Lett.* **96** 119602
[38] Li Y and Chang C R 2004 *J. Magn. Magn. Mater.* **277** 344
[39] Perdew J P and Wang Y 1992 *Phys. Rev.* B **45** 13244
[40] Henk J, Mirhosseini H, Bose P, Saha K, Fomynikh N, Scheunemann T, Halilov S V, Tamura E and Feder R 2007 OMNI2K—*Fully Relativistic Electron Spectroscopy Calculations* The computer code is available from the authors
[41] Henk J 2001 *Handbook of Thin Film Materials* vol 2, ed H S Nalwa (San Diego, CA: Academic) chapter 10, p 479
[42] Zabloudil J, Hammerling R, Szunyogh L and Weinberger P (ed) 2005 *Electron Scattering in Solid Matter* (Berlin: Springer)
[43] MacLaren J M, Zhang X G, Butler W H and Wang X 1999 *Phys. Rev.* B **59** 5470
[44] Zhang X G, Butler W H and Bandyopadhyay A 2003 *Phys. Rev.* B **68** 092402
[45] Belashchenko K D, Tsymbal E Y, van Schilfgaarde M, Stewart D A, Oleinik I I and Jaswal S S 2004 *Phys. Rev.* B **69** 174408
[46] Wortmann D, Bihlmayer G and Blügel S 2004 *J. Phys.: Condens. Matter* **16** S5819
[47] Heiliger C, Zahn P, Yavorsky B Y and Mertig I 2005 *Phys. Rev.* B **72** 180406(R)
[48] Bose P, Mertig I and Henk J 2007 *Phys. Rev.* B **75** 100402(R)
[49] Slonczewski J C 1989 *Phys. Rev.* B **39** 6995
[50] Rose E M 1961 *Relativistic Electron Theory* (New York: Wiley)
[51] Kessler J 1985 *Polarized Electrons* (*Springer Series on Atoms and Plasmas* vol 1) 2nd edn (Berlin: Springer)
[52] Gao L, Jiang X, Yang S H, Burton J D, Tsymbal E Y and Parkin S S P 2007 *Phys. Rev. Lett.* **99** 226602
[53] Ackermann B, Feder R and Tamura E 1984 *J. Phys. F: Met. Phys.* **14** L173
[54] Sharvin Y Y 1965 *Sov. Phys.—JETP* **21** 655
[55] Devreese J T and Peeters F M (ed) 1987 *The Physics of the Two-Dimensional Electron Gas* (*NATO ASI Series B* vol 157) (New York: Plenum)
[56] Krupin O, Bihlmayer G, Starke K, Gorovikov S, Prieto J E, Döbrich K, Blügel S and Kaindl G 2005 *Phys. Rev.* B **71** 201403(R)
[57] Petersen L and Hedegård P 2000 *Surf. Sci.* **459** 49
[58] Mugarza A, Mascaraque A, Repain V, Rousset S, Altmann K N, Himpsel F J, Koroteev Y M, Chulkov E V, García de Abajo F J and Ortega J E 2002 *Phys. Rev.* B **66** 245419
[59] Yuasa S, Nagahama T and Suzuki Y 2002 *Science* **297** 234
[60] Wunnicke O, Papanikolaou N, Zeller R, Dederichs P H, Drchal V and Kudrnovský J 2002 *Phys. Rev.* B **65** 064425
[61] Mu H F, Zhu Z G, Zheng Q R, Jin B, Wang Z C and Su G 2004 *Phys. Lett.* A **323** 298